Efficiency analysis in the chemical loop process of base metals.

I.Marques-Valderrama[a], J. A Becerra[b], C. Ortiz[c], D. A Rodríguez Pastor[d] and R.Chacartegui[e]

[a] *University of Seville, Seville, Spain, imarques2@us.es*
[b] *University of Seville, Seville, Spain, jabv@us.es*
[c] *University of Seville, Seville, Spain, cortiz7@us.es*
[d] *University of Seville, Seville, Spain, drodriguez4@us.es*
[e] *University of Seville, Seville, Spain, ricardoch@us.es*

Abstract:

This work proposes a thermochemical storage system for Iron, aluminium, and nickel oxidation/reduction reactions. The chemical looping process based on the analysed reaction pairs will involve high energy efficiencies, given their high energy density (40-80 MJ/l) and the contribution of reducing agents such as hydrogen and carbon monoxide. The mix of these reductor agents is considered according to the Baur-Glassner diagram. In the charging process, it will make use of renewable energy sources (CSP+PV) to carry out the decomposition process (570°C or lower, depending on the number of stages in the reduction in the iron case). In the discharge phase (800°C depending on the metal and the particle radius), the reduced metal passes through a combustion chamber where it is oxidised, generating thermal energy useful for other processes, and obtaining metal oxides that will serve to close the proposed cycle. The temperatures required in the charge/discharge processes by the different metals have been studied, including an analysis of the energy integration of the different equipment and heat for processes. The simulations were carried out in the commercial software EES to evaluate the more suitable metals to obtain the reductant. a Round Trip Efficiency study has been carried out to evaluate the different TCES configurations.

Keywords:

Thermochemical storage, Chemical looping, Hydrogen, Energy integration, Round Trip Efficiency.

1. Introduction

Reducing dependence on carbon sources meeting the growing energy demand of society [1], is together with climate change one of the main challenges facing the world today [2]. One of the current lines of greatest development is energy storage. Have systems that take advantage of the surplus energy production offered by other facilities to be used later.Developing low-carbon energy carriers has become crucial for reducing dependence on fossil fuels in energy production and distribution. This, together with other fundamental aspects of decarbonization and the use of renewables, leads to the search for cost-efficient energy storage systems. Energy storage is crucial for a market with a high presence of renewable generation. To increase the availability of renewable generation and increase the inertia of the grid. One of the main advantages of energy storage is the possibility of designing renewable facilities of greater capacity, improving their inertia in the electricity grid [3]. Parameters for the competitiveness of renewable energies.

Different types of energy can be stored depending on the systems to which they are linked [4] and the form in which the energy is stored/released: chemical, electrical, magnetic, electrochemical, mechanical, and thermal storage systems [5]. The use of these systems supports installations to produce electricity.Metal oxides can be integrated as energy storage systems [6]. These materials have been studied from the electrical point of view, to be used directly in batteries. Recently, they have been studied as regenerative fuel sources [7], in reactors with metals as a fuel source, taking advantage of the thermal energy generated in the oxidation process [8]. It arises because of the high energy density of these materials, which require a lower fuel volume, availability, and regenerative capacity. The iron powder has been tested in the MP100 reactor developed by the University of Eindhoven [9]. There are possibilities for considering the use of a series of metals for this application. Based on the development of these reactors, it is feasible to create a thermochemical storage system based on metals, obtaining thermal energy from their oxidation. Regeneration of the reduced metal from different metal oxides can be obtained in elements such as nickel [10] or iron [9] from reducing agents such as Hydrogen or Carbon Monoxide [11]. Having identified the possibility of integration of these systems,

https://doi.org/10.52202/069564-0212

this work analyses different configurations of thermochemical storage systems, analysing their potential as energy storage systems [11] and their potential to advance in this line.

2. State of the art

2.1. Energy storage based on metals

Metals have high energy densities when compared to other types of fuels. The graph below shows the gravimetric energy density [MJ/kg] versus the volumetric energy density [MJ/L] of a wide range of fuels used today.

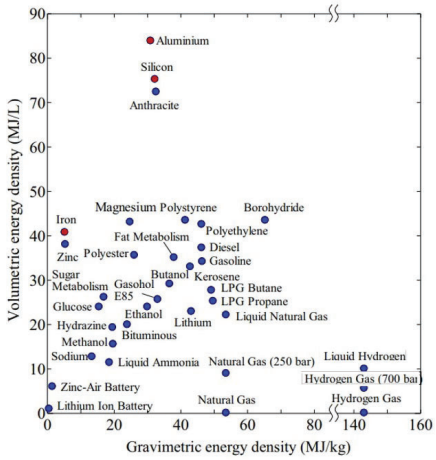

Figure. 1. Gravimetric energy density versus volumetric energy density of different fuels.[8]

Figure 1 shows a number of metals with high volumetric energy densities, like Iron, providing the opportunity of reducing the required volume for an energy design and smaller equipment if used in oxidation/combustion processes. Figure 1 shows the main metals studied. This study also will address the use of Nickel, that is not included in Figure 1 [8]. Their use in an energy storage system considers a closed chemical looping system, operating sequentially on loading and discharging stages, where the metal is oxidised and regenerated. The metals subjected to the oxidation/combustion process will form the discharge system. The metal oxides formed in the process will be stored in the loading system, from which the initial fuel will be regenerated from a reduction process [13]. Figure 2 shows a general operating scheme that has been proposed that will be used for assessing the use of different metals:

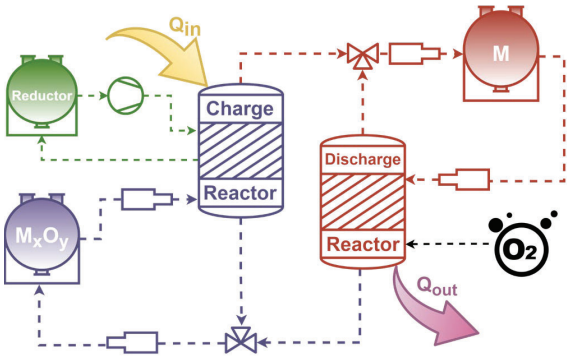

Figure. 2. General diagram of the storage system.

The cycle is divided into two main blocks/reactors:

- Charging system: Consists of two subsystems. The storage and management of metal oxide and the management of the reducer to reconvert the product of the discharge into fuel.
- Discharging system: Management of the storage and oxidation of the original fuel in the discharge reactor.

https://doi.org/10.52202/069564-0212

For the operation of the loading system, two possible reducers will be considered: carbon monoxide as a reductant as a product of synthesis gasification and hydrogen. This hydrogen can be produced within the gasification or by electrolysis powered by photovoltaic or wind energy. The selected metals to analyse the concept were Fe, Al, and Ni.

2.3. State diagrams

2.3. 1 Charging process

Departing with the charging process, integrating a metal oxide and a reducer generates a reduced metal. The reaction requires appropriate temperature and reaction conditions. In this work, Fe and Ni have been considered. To identify their behaviour and evolution under different conditions, their state diagrams graphs were modelled in the FactSage program for the following combinations of metals and reducers:

Table 1. Generated status diagrams.

Chart No.	Process	Elements evaluated
1	Reduction	Fe – H_2 – H_2O Fe – CO – CO_2
2	Reduction	Al – H_2 – H_2O Al – CO – CO_2
3	Reduction	Ni – H_2 – H_2O Ni – CO – CO_2
4	Oxidation	Fe – O_2
5	Oxidation	Al – O_2
6	Oxidation	Ni – O_2

The elements were included using the FactPs and FToxid databases [12] These state diagrams provide guidelines about phase equilibria temperatures depending on the amount of oxidiser or reductant in the reactors. In this environment, metals, their oxides, oxygen, reducers, and their products are considered. These graphs provide the temperatures for reducing metal oxides as a function of the minimum metal fraction and the operating atmospheres of CO / CO_2 and H_2 / H_2O [13]. Different reduction processes of iron oxide are considered for the generation of DRI (Direct Reduced Iron) [14]. The Bauer-Glaessner diagram can be used to [10] compare the reducer's concentrations and process temperatures using Carbon Monoxide and Hydrogen [11]. The curves for the case of Aluminum and Nickel used in this study obtained using FactSage, are presented in Figure 3.

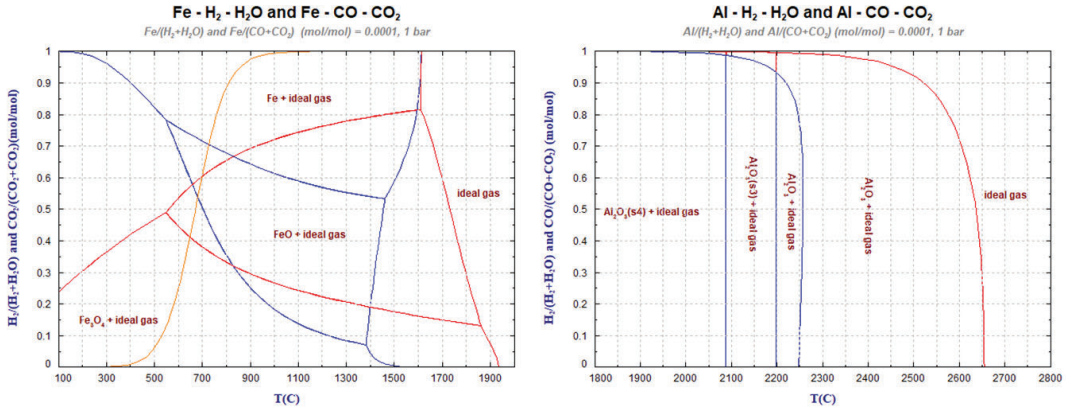

Figure. 3. Comparison of temperatures in the reduction of oxides of Iron and Aluminum.

2.2.3 Discharging process

The oxidation process is studied for the selected metals. The Figure 4 represents the equilibrium curves and metal concentration in all cases.

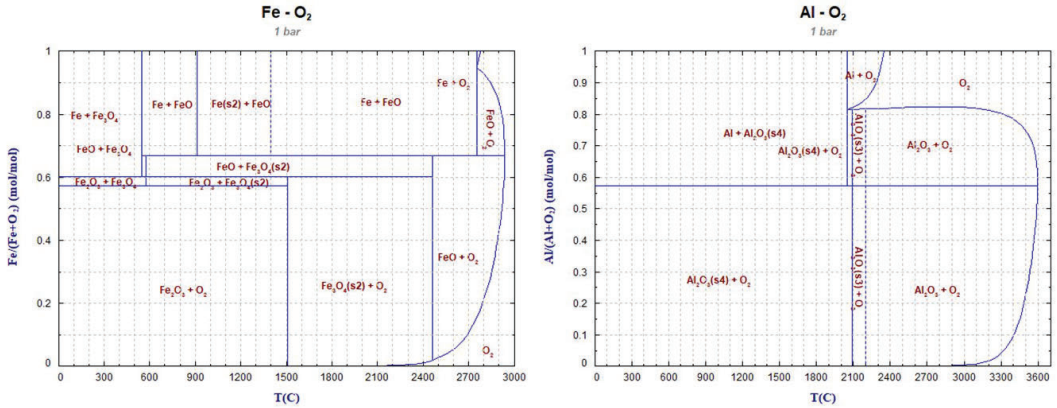

Figure. 4. Comparison of temperatures in the oxidation of Iron, Aluminum and Nickel.

The analysis of gigures 3 and 4 shows seen how in the case of Iron and Aluminum, different metal oxides can be obtained depending on the reaction temperature and the proportion of metal and oxidiser. On the other hand, it is also observed that in the reduction processes, depending on the metal chosen, a different amount of reducer is required if Hydrogen or Monoxide is chosen as a reducing agent.

2.3.4 Reducer mixtures

As can be seen in the case of Iron, reducer concentrations mark different equilibrium curves. For mixtures of CO and H_2, as in the case of syngases, the resulting equilibrium curve will be between the two represented in the diagram, in a phase diagram with intermediate states that depend on the concentration of the reducer mixture, Figure 5.

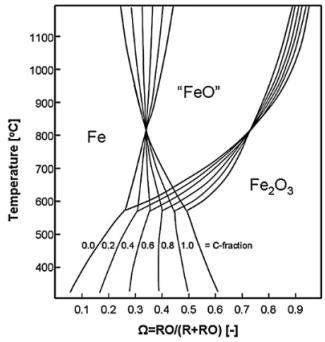

Figure. 5. Baur-Glaessner diagram for CO-H2 mixtures as reducing agent.[14]

It is observed how the equilibrium curves are distributed between the two extreme cases depending on the concentration of reducers in the mixture and the amount of monoxide present. Therefore, regarding the proposed charging system, cases have been studied in which only Hydrogen or Carbon Monoxide is available as a reducer agent. The reducer management schemes in both cases could be as presented in Figure 6:

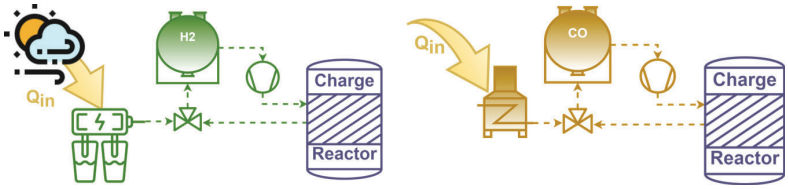

Figure. 6. Possible operating schemes for the reducing agent.

2.3.2 Activation energies

A relevant aspect is the activation energy of the reactions. It will penalise the available energy, both in the case of the charge and the discharge. The energy needed to activate the process will depend, among other factors, on the kinetics of each reaction. The dependencies of variables depend on each reaction. Accurate information can be obtained by measuring the concentrations through thermogravimetric analyses. Based on the experimental results of the specific results, methods such as Kissinger's are used [15] to determine the kinetic characteristics of the reaction. The activation energies of the following reactions are identified in the literature:

https://doi.org/10.52202/069564-0212

Table 2. Activation energies.

Reaction	Mechanism	Minimum [kJ/mol]	Maximum [kJ/mol]
$NiO(s) + H_2(g) \rightleftarrows Ni\ (s) + H_2O\ (g)$	Reduction	85 [16]	126 [16]
$Ni(s) + \frac{1}{2}\ O_2(g) \rightleftarrows NiO$	Oxidation	172,38 [17]	209,2 [17]
$3Fe(s) + 2O_2(g) \rightleftarrows Fe_3O_4(s)$ below 570°C	Oxidation	130 [18]	170 [18]
$3Fe_2O_3(s) + 4H_2(g) \rightleftarrows 2Fe_3O_4(s) + 4H_2O_{(g)}$	Reduction	89,1 [19]	282 [20]
$Fe_3O_4(s) + 4H_2(g) \rightleftarrows 3Fe(s) + 4H_2O_{(g)}$	Reduction	54,0 [19]	167 [21]
$2Fe(s) + \frac{3}{2}O_2(g) \rightleftarrows Fe_2O_3(s)$	Oxidation	110 [22]	
$Fe_3O_4(s) + H_2(g) \rightleftarrows 3FeO(s) + H_2O_{(g)}$	Reduction	47 [23]	
$FeO\ (s) + H_2(g) \rightleftarrows Fe\ (s) + H_2O_{(g)}$	Reduction	30 [23]	

To determine the power of the use of the metals selected for the described application, a theoretical Round-Trip Efficiency (RTE) [24] is defined [25]. It determines the energy recovery potential of the system at different operating temperatures, equation 1.

$$\eta_{RTE} = \frac{Q_{Av}}{Q_N} = \frac{\left|Q_{disc} + E_A^{Disch}\right|}{\left|Q_{ch} + E_A^{ch}\right|} \tag{1}$$

Where Q_{Av} refers to the energy per mole of fuel available in the discharge process. This is determined from the discharge energy per mole of fuel obtained, Q_{disc} minus the activation energy term needed to start the process E_A^{Disch}. The same reasoning is applied to the charging process, Q_N where Q_{ch} is the energy per mole of fuel necessary for the reduction of the metal oxides studied and refers to the term of activation energy necessary to start the charging process E_A^{ch}, Figure 7.

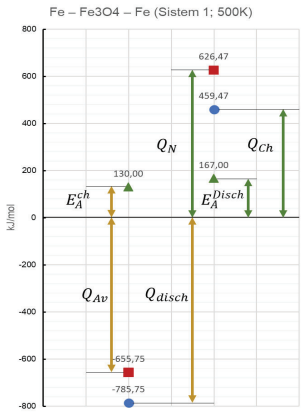

Figure. 7. Theoretical Round Trip Efficiency of Iron.

3. Results and discussion

3.1. Description of the system

Considering the layout in Figure 2, two sources have been taken to obtain the reducer. First, there is the possibility of using hydrogen from electrolysis. This process will be powered by a photovoltaic solar installation. On the other hand, the production of carbon monoxide through gasification from synthesis is proposed.

3.2. Calculation of properties

For the analysis of the different configurations, metals and potential metal oxides, a series of models have been implemented in OpenModelica [26], [27]. An OpenModelica library for the calculation of thermodynamic properties has been implemented based on Glenn coefficients[28], equations 2 to 4.

$$\frac{c_p^{\circ}(T)}{R} = a_1T^{-2} + a_2T^{-1} + a_3 + a_4T + a_5T^2 + a_6T^3 + a_7T^4 \tag{2}$$

$$\frac{h°(T)}{RT} = -a_1T^{-2} + a_2\frac{lnT}{T} + a_3 + a_4\frac{T}{2} + a_5\frac{T^2}{3} + a_6\frac{T^3}{4} + a_7\frac{T^4}{5} + b_1T^{-1} \tag{3}$$

$$\frac{s°(T)}{R} = -a_1\frac{T^{-2}}{2} - a_2T^{-1} + a_3lnT + a_4T + a_5\frac{T^2}{2} + a_6\frac{T^3}{3} + a_7\frac{T^4}{2} + b_2 \quad (4)$$

Using the coefficients by intervals for each element/substance, the demands and energy released in the loading and unloading processes can be calculated [29]. The "Equilibrium" module included in FactSage has been used, as well as the [30] Chemical Equilibrium Applications (CEA), for the verification of the calculation of the properties[31], [28]. A second library was generated aimed at performing energy analysis of the charge/discharge processes where the enthalpies of the reaction and Gibbs free energy of all processes were calculated.

$$h_{reac} = \sum n_P \cdot \Delta h(T)_{,P} - \sum n_R \cdot \Delta h(T)_{,R} \quad (5)$$

$$g = \Delta h - T\Delta s \quad (6)$$

The reaction enthalpies were calculated based on the moles of metal in the reactors. In this way, the molar mass, the energy demand of the charging process, and the amount of energy of the discharge process produced per kilogram of metal can be calculated.

3.3. Discharging process

The processes modelled for the discharge of the thermochemical system are presented in Table 3

Table 3.- Discharge reactions considered.

$$2Fe(s) + O_2(g) \rightleftarrows 2FeO(s) \quad (6)$$

$$2Fe(s) + \frac{3}{2}O_2(g) \rightleftarrows Fe_2O_3(s) \quad (7)$$

$$3Fe(s) + 2O_2(g) \rightleftarrows Fe_3O_4(s) \quad (8)$$

$$2Al(s) + \frac{3}{2}O_2(g) \rightleftarrows Al_2O_3(s) \quad (9)$$

$$Ni(s) + \frac{1}{2}O_2(g) \rightleftarrows NiO \quad (10)$$

The models performed simultaneous calculations within a temperature range from 300K to 3600K. This range was selected based on the analysis of phase diagrams.

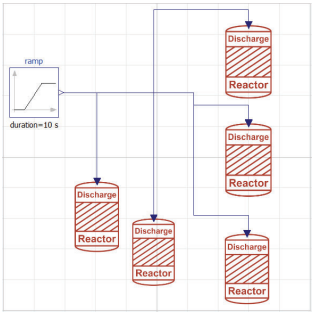

Figure 8.- OpenModelica graphical representation of reactor models.

Graph 4, 5 and 6 shows the enthalpy and Gibbs free energy curves for the different reactions resulting from the simulations.

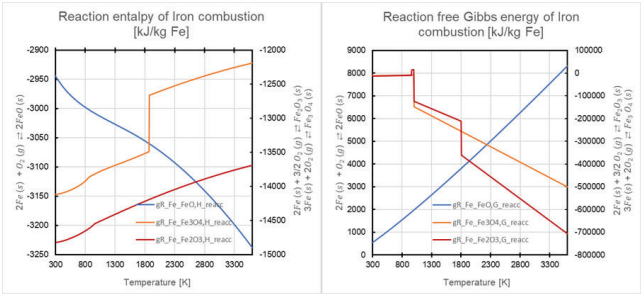

Graph1.- Enthalpy of reaction and Gibbs free energy for possible oxidation reactions of Iron.

https://doi.org/10.52202/069564-0212

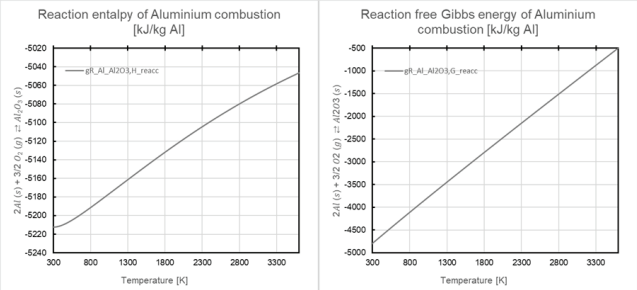

Graph2.- Enthalpy of reaction and Gibbs free energy for the oxidation of Aluminum.

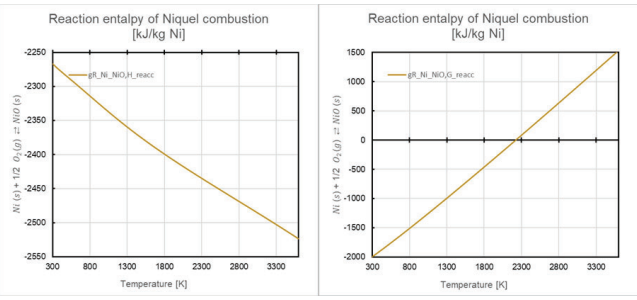

Graph3.- Enthalpy of reaction and Gibbs free energy for the oxidation of Nickel.

The variation of the power obtained per kilogram of fuel is observed in temperatures ranging from 300K to 3600K. They show the high energy potential of these metals as fuels in oxidising processes. On the other hand, within the oxidation reactions studied for the case of Iron, it is known according to literature that the majority product generated in the oxidation process can be Hematite or Magnetite depending on the conditions.

3.4. Charging processes

In the charging process the reactions evaluated are presented in Table 4:

Table 4.- Charge reactions considered.

$$3Fe_2O_3(s) + 4H_2(g) \rightleftarrows 2Fe_3O_4(s) + 4H_2O_{(g)}$$
$$Fe_3O_4(s) + H_2(g) \rightleftarrows 3FeO(s) + H_2O_{(g)} \quad (11)$$
$$FeO\ (s) + H_2(g) \rightleftarrows Fe\ (s) + H_2O_{(g)}$$

$$3Fe_2O_3(s) + CO(g) \rightleftarrows 2Fe_3O_4(s) + CO_2(g)$$
$$Fe_3O_4(s) + CO\ (g) \rightleftarrows 3FeO\ (s) + CO_2(g) \quad (12)$$
$$FeO\ (s) + CO\ (g) \rightleftarrows Fe\ (s) + CO_2(g)$$

$$Fe_3O_4(s) + 4H_2(g) \rightleftarrows 3Fe\ (s) + 4H_2O(g) \quad (13)$$
$$Fe_3O_4(s) + 4CO(g) \rightleftarrows 3Fe(s) + 4CO_2(g) \quad (14)$$
$$NiO(s) + H_2(g) \rightleftarrows Ni\ (s) + H_2O\ (g) \quad (15)$$
$$NiO(s) + CO(g) \rightleftarrows Ni\ (s) + CO_2\ (g) \quad (16)$$
$$Al_2O_3(s) + 3H_2(g) \rightleftarrows 2Al\ (s) + 3H_2O\ (g) \quad (17)$$
$$Al_2O_3(s) + 3CO(g) \rightleftarrows 2Al\ (s) + 3CO_2\ (g) \quad (18)$$

Two different paths have been identified for the reduction of Magnetite (Fe_3O_4),since if it is reduced to a temperature lower than 843K, the reduction occurs directly without passing through the state of Wüstite (FeO), as observed in Figure 3, It should also be noted within the initial scope of this study, Hydrogen, and Carbon Monoxide have been chosen as reductants, but the use of combinations of metals in the reduction process that requires a lower amount of energy in the process can be studied.

3.4.1. Reduction of F2O3 to Fe at temperatures above 843K

For temperatures above 570K the reduction of Hematite is done in three steps. First, it is reduced to Magnetite (Fe3O4). Subsequently, increasing the concentration of the reducer is passed from Magnetite to Wüstite (FeO). Finally, it is reduced to Iron. This 3-phase process has some interesting characteristics when compared

to the loading processes of systems with Nickel or Aluminum since, depending on the operating conditions, up to two exothermic phases can be achieved, corresponding to the reduction of Hematite and Wüstite.

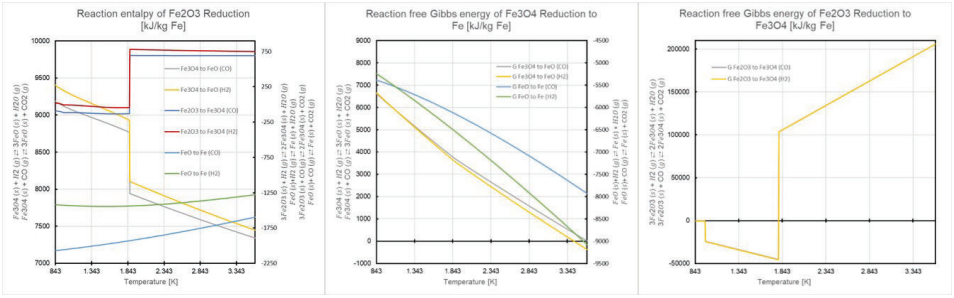

Graph4.- Enthalpy and Gibbs free energy for the reduction of Hematite to Iron at temperatures greater than 843K.

It is observed that, in the first step of the process, the reduction of Hematite to Magnetite is spontaneous between 843K and 1800K. From that temperature, the equilibrium between phases is not given[12]. On the other hand, in the overall balance of the reduction, having the same temperature for all phases, the following process demand is obtained depending on the operating temperature:

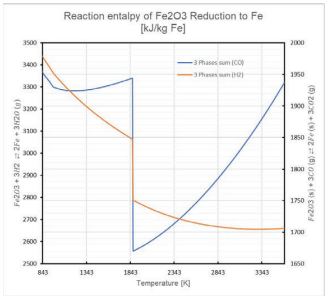

Graph5.- Total loading process in the reduction of Hematite at temperatures above 843K.

It is observed how this configuration offers a variety of configurations where lower demands can be obtained than those shown if adequate temperatures of reduction of Hematite and Wüstite are chosen. In the same way, this demand can be reduced according to the reducer chosen in each phase.

3.4.2. Reduction of F2O3 to Fe at temperatures below 843K

In this case, the reduction occurs directly from the Magnetite phase to Iron. Therefore, the charging system would have two phases. An initial phase in which the Hematite is reduced obtaining Magnetite, and a final phase in which the Magnetite is reduced directly to Iron. This system, as in the previous one, can be operated at different temperatures depending on the phase being studied, so the system can operate as follows:

- The first phase can occur at any temperature, provided that the product obtained is Magnetite.
- Once Magnetite is obtained as a product, it is passed to a temperature within the study range. Process heat will be obtained from the temperature reduction.
- When the temperature of the Magnetite is lower than the 843K that has been marked as a limit, the reduction to Iron is made.

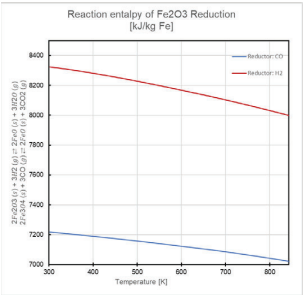

Graph 9.-6 Total loading process in the reduction of Hematite at temperatures below 843K.

https://doi.org/10.52202/069564-0212

3.4.2. Reduction from NiO to Ni

For this system of cages, the demand for the reduction process per kilogram of Nickel has been studied. In this case, as in the previous ones, the reduction has been compared using Hydrogen and Carbon Monoxide as reducers.

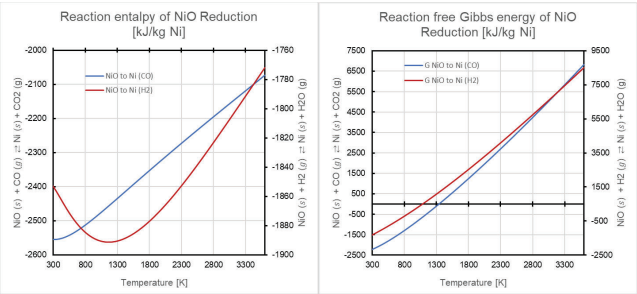

Graph7.- Enthalpy and Gibbs free energy in the reduction of NiO to Ni.

3.4.2. Reduction of Al2O3 to Al

In the charging system corresponding to obtaining reduced Aluminum, the same approach has been followed as in the case of nickel, making a temperature analysis with the two reducers chosen. Taking this into account, the demand for the reduction of 1kg of Aluminum would be as follows:

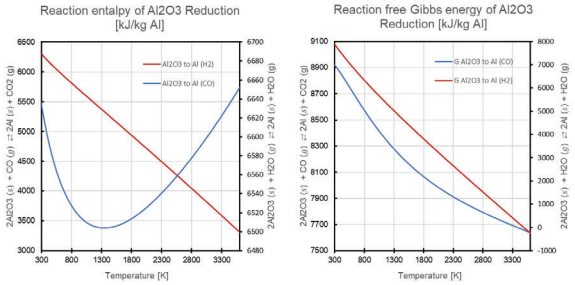

Graph8.- Enthalpy and Gibbs free energy in the reduction of Al2O3 to Al.

3.4. Energy Storage Layouts

The energy storage layouts and processes are presented following the layout presented in ***Figure* 2,** *with* different configurations depending on the metal used, and in the case of Iron, depending on the temperature of reduction of Magnetite Three different systems are proposed:

- System 1: In the case of working with Nickel or Aluminum.
- System 2: In the case of working with Iron and carrying out the reduction of Magnetite to a temperature below 873K. It will have two charge stages.
- System 3: For the case in which you work with Iron, the magnetite reduction process is carried out in 2 stages, forming Wüstite in phase 2.

The general operating schemes of the different configurations presented would be as follows:

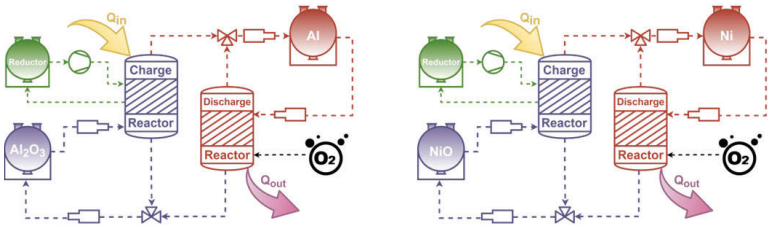

Figure 9.- Operating scheme type 1 charge / 1 discharge.

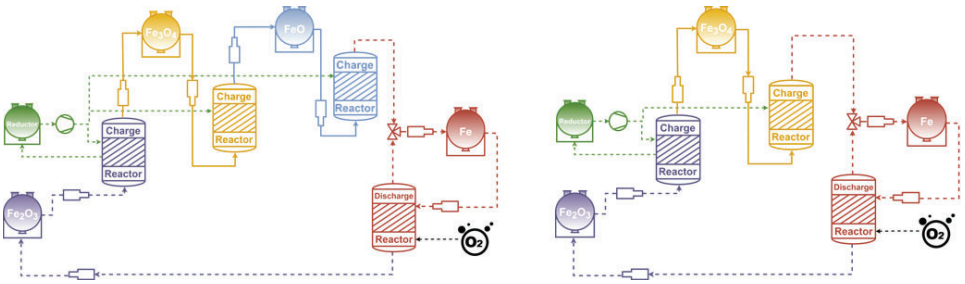

Figure 10.- Operating scheme type 1 charge / 2 discharges, and operating scheme (2 charges/ 1 discharge).

For the operating schemes in the case of Iron, the tanks defined as charge, in the case of the reduction of hematite will demand or offer energy to the system depending on the operating conditions that define the process.

3.5. Performance

This section makes ana preliminary study of the performance of the systems based on their Round-Trip Efficiencies. The same temperature has been considered for the charging and discharge processes, although any other could have been selected. The viability of the process and the RTE have a strong dependence on the reaction's evolution.

Table 5.-5 Results of RTE at different temperatures.

Temperature [K]	Metal	System	RTE	Notes
500	Fe	2	78,83%	Oxidation to Fe2O3, reduction by H2
800	Fe	3	78,92%	Oxidation to Fe2O3, reduction by H2
1100	Fe	3	87,89%	Oxidation to Fe2O3, reduction by H2

The description of the type of system in the table can be found in section 3.4.

Once the graphs relating to the selected metals have been presented, and an RTE has been proposed for iron-based systems (due to having a wider and more reliable amount of information in these reactions), it can be observed how for ranges between 500K and 1800K, the oxidation processes of the three metals studied have an energy potential that can range since 2.4 MJ/kg in the case of Nickel to 5 MJ/Kg in the case of Aluminum. These results have been obtained under the assumption of complete conversion. As presented in [7], it is also verified that the work of the discharge system in the range of the proposed temperatures is possible. On the charging process side, the amount of energy required and the possibility of performing the reduction depending on the mechanism employed. It is verified that there are cases in which the most favorable reducing agent (energetically) is carbon monoxide, where differences of up to 1MJ / Kg of reduced metal can be found compared to using hydrogen as a reducing agent. On the other hand, taking into account the state diagrams presented in Figure 3, it is observed that the reduction process is more favorable energetically at certain temperatures, being usually more favorable when increasing the temperature of the process. The energy required in the reduction processes as a function of temperature is different for the three metals due to the stability of the phases. In terms of activation energies necessary for the processes, several sources in the literature have been evaluated, and those for which more information was available under the conditions that have been studied have been chosen for the initial estimation of the RTE. It is observed how the importance of determining the conditions in which the charging process will take place is vital to minimize the activation energies. It was considered that taking into account the conditions under which the activation energies were determined, those used for the determination of the RTE would be the ones of greater value, even considering that, for the reactions studied, these values may be higher. Finally, it is observed that the values of RTE vary between 78% and 88%.

4. Conclusions

This work presents a preliminary analysis of metal-based energy storage systems. The energy potential of these types of reactions raises the modality of the proposed thermochemical storage system. The analysis in a wide range of temperatures shows how there are conditions for charge and discharge reactions, which make using metals as a thermochemical storage base possible. The systems were modelled in an OpenModelica library. It has been assembled where the entire modelling process has been carried out, from the properties of the materials to the study of the reactions. This library is designed to be able to make comparisons with laboratory tests and will serve as support for the study of this storage system.

https://doi.org/10.52202/069564-0212

The analyses show the feasibility and potential of the proposed energy storage layouts. Taking into account the range of working temperatures, it opens the possibility of integrating these facilities in processes with high thermal production, increasing the energy integration of existing facilities with the possibility of energy recovery. The analyses show how activation energies for the specific working conditions affect the round-trip efficiency values.

For this proposal of thermochemical energy storage based on the combustion of metals, the interest that the use of this type of materials as fuel can offer is observed. Among the points raised in this article, different lines of study are opened that will have this concept as a starting point. They include the study of the integration of green hydrogen production facilities from photovoltaic solar energy in this system, as well as carbon monoxide production plants and energy integration of the system depending on the chosen configuration.

Acknowledgments

This work has been partially developed within the project, New modular high-temperature thermo-chemical energy storage concept based on innovative processes (TED2021-131839B-C21) funded by the Recovery and Resilience Funds of the European Union and Spanish Ministry of Science and Innovation.

Nomenclature

Fe	Iron	
Fe_2O_3	Hematite	
Fe_3O_4	Magnetite	
FeO	Wüstite	
Al	Aluminium	
Al_2O_3	Aluminum Oxide	
Ni	Nickel	
NiO	Nickel (II) oxide	
CO	Carbon monoxide	
H_2	Hydrogen	
CO_2	Carbon Dioxide	
H_2O	Water	
c_p	Heat capacity	[kJ/(kg·K)]
h	Especific enthalpy	[kJ/kg (fuel)]
s	Especific entropy	[kJ/(mol·K)]
g	Gibbs free energy	[kJ/kg (fuel)]
RTE	Round Trip Efficiency	[-]

References

[1] "Estadísticas de consumo energético mundial | Enerdata." https://datos.enerdata.net/energia-total/datos-consumo-internacional.html (accessed Apr. 24, 2023).

[2] U. Nations, "Global Issues | Naciones Unidas", Accessed: Apr. 24, 2023. [Online]. Available: https://www.un.org/es/global-issues

[3] "e-REdING. Biblioteca de la Escuela Superior de Ingenieros de Sevilla." https://biblus.us.es/bibing/proyectos/abreproy/5641 (accessed Apr. 24, 2023).

[4] I. Hadjipaschalis, A. Poullikkas, and V. Efthimiou, "Overview of current and future energy storage technologies for electric power applications", doi: 10.1016/j.rser.2008.09.028.

[5] "Technologies | EASE: Why Energy Storage? | EASE." https://ease-storage.eu/energy-storage/technologies/ (accessed Apr. 24, 2023).

[6] Y. Wang *et al.*, "Application of MOFs-derived mixed metal oxides in energy storage," *Journal of Electroanalytical Chemistry*, vol. 878, p. 114576, Dec. 2020, doi: 10.1016/J.JELECHEM.2020.114576.

[7] "La primera cervecería en quemar hierro como energía verde es holandesa | IKERA." https://ikera.es/la-primera-cerveceria-en-quemar-hierro-como-energia-verde-es-holandesa/ (accessed Apr. 24, 2023).

[8] "J. Bergthorson, McGill University - Metal Fuels for Compact Zero-carbon Power - YouTube." https://www.youtube.com/watch?v=VjCGXxFHGcw (accessed May 31, 2022).

[9] “Mapping Temperature Characteristics of Iron Powder Combustion in the MP100 Setup — Eindhoven University of Technology research portal.” https://research.tue.nl/en/studentTheses/mapping-temperature-characteristics-of-iron-powder-combustion-in- (accessed Apr. 24, 2023).

[10] K. V Manukyan *et al.*, “Nickel Oxide Reduction by Hydrogen: Kinetics and Structural Transformations,” *J. Phys. Chem. C*, vol. 119, p. 42, 2015, doi: 10.1021/acs.jpcc.5b04313.

[11] A. Carlos, G. Tello, P. Jaime, L. Mateo, J. Ángel, and P. Llorente, “PURIFICACIÓN DE MEZCLAS H 2-CO 2 MEDIANTE EL PROCESO ‘STEAM-IRON’ CON ÓXIDOS DE HIERRO,” 2016.

[12] “Phase Diagram The Phase Diagram module 1.2”, Accessed: Mar. 25, 2023. [Online]. Available: www.factsage.com

[13] “Use el módulo de diagrama de fase Diagrama de fase de FactSage para dibujar el diagrama de equilibrio del sistema Fe-OC.” https://zhuanlan.zhihu.com/p/419199865 (accessed Mar. 25, 2023).

[14] L. Kolbeinsen, “Modelling of DRI processes with two simultaneously active reducing gases,” *Steel Res Int*, vol. 81, no. 10, pp. 819–828, Oct. 2010, doi: 10.1002/SRIN.201000144.

[15] S. Vyazovkin, “Kissinger Method in Kinetics of Materials: Things to Beware and Be Aware of,” *Molecules 2020, Vol. 25, Page 2813*, vol. 25, no. 12, p. 2813, Jun. 2020, doi: 10.3390/MOLECULES25122813.

[16] J. T. Richardson, R. Scates, and M. V Twigg, “X-ray diffraction study of nickel oxide reduction by hydrogen,” 2003, doi: 10.1016/S0926-860X(02)00669-5.

[17] J. P. Baur, R. W. Bartlett, J. N. Ong, and W. M. Fassell, “High-Pressure Oxidation of Metals, Nickel in Oxygen”.

[18] L. del Campo, R. B. Pérez-Sáez, and M. J. Tello, “Iron oxidation kinetics study by using infrared spectral emissivity measurements below 570 °C,” *Corros Sci*, vol. 50, no. 1, pp. 194–199, Jan. 2008, doi: 10.1016/J.CORSCI.2007.05.029.

[19] A. Pineau, N. Kanari, and I. Gaballah, “Kinetics of reduction of iron oxides by H2: Part I: Low temperature reduction of hematite,” *Thermochim Acta*, vol. 447, no. 1, pp. 89–100, Aug. 2006, doi: 10.1016/J.TCA.2005.10.004.

[20] C. Kuhn, A. Düll, P. Rohlfs, S. Tischer, M. Börnhorst, and O. Deutschmann, “Iron as recyclable energy carrier: Feasibility study and kinetic analysis of iron oxide reduction,” *Applications in Energy and Combustion Science*, vol. 12, p. 100096, Dec. 2022, doi: 10.1016/J.JAECS.2022.100096.

[21] A. Pineau, N. Kanari, and I. Gaballah, “Kinetics of reduction of iron oxides by H2: Part II. Low temperature reduction of magnetite,” *Thermochim Acta*, vol. 456, no. 2, pp. 75–88, May 2007, doi: 10.1016/J.TCA.2007.01.014.

[22] E. N. Lysenko, • A P Surzhikov, • S P Zhuravkov, V. A. Vlasov, • A V Pustovalov, and N. A. Yavorovsky, “The oxidation kinetics study of ultrafine iron powders by thermogravimetric analysis”, doi: 10.1007/s10973-013-3456-x.

[23] A. A. Barde, J. F. Klausner, and R. Mei, “Solid state reaction kinetics of iron oxide reduction using hydrogen as a reducing agent,” *Int J Hydrogen Energy*, vol. 41, no. 24, pp. 10103–10119, Jun. 2016, doi: 10.1016/J.IJHYDENE.2015.12.129.

[24] “IEEE Xplore Full-Text PDF:” https://ieeexplore.ieee.org/stamp/stamp.jsp?tp=&arnumber=8738863 (accessed Apr. 13, 2023).

[25] Y. Zhang and Z. Yang, “Comparative study on optimized round-trip efficiency of pumped thermal and pumped cryogenic electricity storages,” *Energy Convers Manag*, vol. 238, p. 114182, Jun. 2021, doi: 10.1016/J.ENCONMAN.2021.114182.

[26] “JModelica.org User Guide Version 2.4 JModelica.org User Guide: Version 2.4,” 2018.

[27] P. A. Fritzson, *Introduction to modeling and simulation of technical and physical systems with Modelica*. Wiley, 2011.

[28] B. J. Mcbride, M. J. Zehe, and S. Gordon, “NASA Glenn Coefficients for Calculating Thermodynamic Properties of Individual Species,” 2002, Accessed: Mar. 21, 2023. [Online]. Available: http://www.sti.nasa.gov

[29] B. J. Mcbride, S. Gordon, and A. Cleveland, “NASA Reference Computer Program for Calculating and Fitting Thermodynamic Functions,” 1271.

[30] “EquiSage”.

[31] M. J. Zehe, S. Gordon, and B. J. Mcbride, “CAP: A Computer Code for Generating Tabular Thermodynamic Functions from NASA Lewis Coefficients,” 2002, Accessed: Mar. 25, 2023. [Online]. Available: http://www.sti.nasa.gov

 https://doi.org/10.52202/069564-0212